Research in Astronomy and Astrophysics manuscript no.
(LaTeX: main.tex; printed on January 18, 2020; 10:37)

Long-term Analysis of Clear Nights Using Satellite Data Considering Astronomical Sites in Western China ⋆

Zi-Huang Cao[1,2], Li-Yong Liu[1], Yong-Heng Zhao[1,2], Lu Feng[1], Hugh R. A. Jones[4], Huang Shen[5], Jin-Xin Hao[1], Yan-Jie Xue[1], Yong-Qiang Yao[1], Jing Xu[2,6], Ali Esamdin[2,6], Zhao-Xiang Qi[2,3], Jian-Rong Shi[1,2], Jian Li[1], Yuan Tian[1], Zheng Wang[1,2], Tai-Sheng Yan[2], Xia Wang[1], Jian-Ping Xiong[2], Jun-Bo Zhang[1], Zhi-Xia Shen[1], Jia Yin[1], Guang-Xin Pu[6], Peng Wei[6], Chun-Hai Bai[2,6], Guo-Jie Feng[2,6], Lu Ma[6], Teng-Fei Song[7], Jian-Feng Wang[1], Jian-Feng Tian[1], Xian-Qun Zeng[1], Zhi-Gang Hou[1], Shi-Long Liao[2], Dong-Wei Fan[1], Yun-Fei Xu[1,2], Chang-Hua Li[1], Yi-Han Tao[1], Si-Cheng Yu[1] and Zhi-Song Cao[1]

[1] National Astronomical Observatories, Chinese Academy of Sciences, Datun Road 20A, Beijing 100101, China

[2] University of Chinese Academy of Sciences, Beijing 100049, China

[3] Shanghai Astronomical Observatory, Chinese Academy of Sciences, Nan Dan Lu 80, Shanghai 200030, China

[4] Centre for Astrophysics, University of Hertfordshire, Hatfield, UK

[5] School of Journalism, Communication University of China, Beijing 100024, China

[6] Xinjiang Astronomical Observatory, Chinese Academy of Sciences, 150 Science 1-Street, Urumqi 830011, China

[7] Yunnan Observatories, Chinese Academy of Sciences, Yang Fang Wang 396, Kunming 650216, China

Abstract A large ground-based optical/infrared telescope is being planned for a world-class astronomical site in China. The cloud-free night percentage is the primary meteorological element for evaluation of the sites. The data from satellites GMS, NOAA, and MODIS were used in this research, covering the period from 1996 to 2015. Our data analysis benefits from overlapping results from different independent teams as well as a uniform analysis of selected sites using GMS+NOAA data. Although significant ground-based monitoring is needed to validate these findings, we identify three different geographical regions with a high percentage of cloud-free conditions (∼83% on average) slightly lower than the Mauna Kea and Armazones sites (∼85% on average) chosen for the large international projects TMT and ELT respectively.

⋆ zhcao@bao.ac.cn

Our study finds evidence that cloud distributions and the seasonal changes affected by the prevailing westerly winds and summer monsoons reduce the cloud cover in areas affected by the westerlies. This is consistent with the expectations from climate change models and is suggestive that most of the identified sites will have reduced cloud cover in the future.

Key words: methods: statistical, site testing, atmospheric effects, MODIS

1 INTRODUCTION

The Large Optical/Infrared Telescope (Cui et al. 2018) is a proposed ground-based general-purpose telescope with a 12 m aperture and adaptive-optics system. The project has a developed engineering design of the telescope but also the scientific goals, related to the instruments and observation modes. Referring to the experience of the Thirty Metre Telescope (TMT) (Schóck et al. 2011) and the Extremely Large Telescope (ELT) (Melnick & Monnet 2011), the percentage of clear-nights is the most straightforward and high-priority parameter in the site merit function (Schóck et al. 2009). However, the definition of the "clear" is indistinct. The different instruments have different interpretations as to cloud, and furthermore the fraction of photometric time and of "usable" time (spectroscopic) need to be well defined and calibrated with respect to ground-based data in a manner similar to that laid out by Cavazzani et al. (2011).

The definition of "clear" is based on different kinds of measurements at different wavelengths and so has a different meaning in different datasets. In this study, although the definition of "clear" is critical for the processing and analysis, the self-consistency and long-term comparability are also important for all datasets. One method to increase the clarity of results would be to consider clear-sky percentages in day-time as well as night-time. For the satellites, sunlight increases the temperature of the surface, which could affect the results of cloud cover. For ground-based observation, sunlight significant increases the contrast of the cloud edges and the moonlight at night could enhance or weaken the potential for cloud identification depending on apparatus, e.g., naked-eye or all-sky camera. Cavazzani et al. (2015) indicates that the difference between day and night is not significant based on 2003 to 2012 data from MODIS at Paranal, La Silla, and Mt Graham. However, it is important to realise that Cavazzani et al. analysis highlighted the need to adjust the pixel position for Paranal in order not to mix the contribution of ocean and land in the same pixel. On the other hand, at a location with very different geography, Barnes et al. (2016) showed a non-negligible difference from the analysis of Hawaiian Island cloud cover from 2001 to 2011 based on the same satellites. For more reliable results on our less studied sites we only process and compare night-time data.

Our analysis considers a range of different potential sites largely selected based on historical experiments and includes existing observatories. Most of the sites are located west of 100° E and north of 40° N. The site altitudes are mostly higher than 4,500 m, and all sites are on the mountain or highland hundreds of meters above the average of the local altitude. All would appear to be

Table 1 Position, Altitude, and Group are given for all sites referred in this work

Site	Longitude (degree)	Latitude (degree)	Altitude (meter)	Group
Muztagh Ata	74.89676	38.33044	4,526	A
Xiangzi	79.85360	31.86121	4,836	B
Diya	78.99159	31.89757	5,143	B
Ali-F	80.33494	32.15154	5,125	B
Ali-D	80.13346	32.25783	5,292	B
Ali-A	80.02671	32.32573	5,040	B
Payang	83.46912	30.04289	4,600	C
Huoerba	83.03725	30.20617	4,621	C
Daocheng	100.10890	29.10695	4,739	D
Delingha	97.72969	37.37794	3,208	E
Gaomeigu	100.02935	26.69378	3,216	E
Nanshan	87.17952	43.47178	2,067	E
Xinglong	117.57744	40.39555	882	E

feasible sites for locating a large telescope. Expect for the sites in group C all are locations for Chinese Academy of Science All-Sky Cameras and Differential Image Motion Monitors.

In order to facilitate comparison between regions, the reference sites divide into groups based on geographic locations. Nearby sites are grouped together, and existing observatories are all assigned to the last group (E). The order of the groups from A to D is according to longitude from west to east, and the site order in the group is according to latitude from south to north. The information about the sites and groups is listed in Table 1.

The research of night cloud cover from the meteorological stations' climate data had finished by Qian et al. (2012). Two large areas with low cloud cover locate in China as shown in Fig. 1, distinguished by the 35% contour line. These cloud-free areas are roughly consistent with previous analyses, e.g., Huang and Mao (1994) and Zhang et al. (2010). East of the 35% contour line, including part of Inner Mongolia, Hebei province and Northeast China, the wind speed is relatively high, there is more dust weather, and severe light pollution associated with intensive human activities. Furthermore, this situation is getting worse with the rapid development of the Chinese economy. Western China, especially inside the 35% contour line, where there is a relatively high percentage of clear-nights area and low population density, including highlands, the Gobi, desert and mountains. All these areas are suitable for a variety of astronomical observations.

As early as the 1980s, surveys of astronomical sites were concentrated on western China, and four new observatories resulted from those surveys, including the Delingha in Qinghai from 1983 (Tian et al. 2016), Nanshan in Xingjiang from 1991 (Liu et al. 2013), and the Gaomeigu in west Yunnan from 1995 (Chen et al. 2003). The geographical distribution of these sites is from 87° E to 101° E, and the altitudes of these sites are from 2,067 to 3,216 m above the sea level, systematically further west and higher than previously existing observatories in China like Xinglong (Zhang et al. 2015). Thus, these observatories serve as a comparative sample for further site-testing. The contours of all our sites are plotted in Fig. 1. The remainder of this paper is arranged as follows.

The description, processing, and results of the satellite data are covered in Section 2, Section 3 concludes our work.

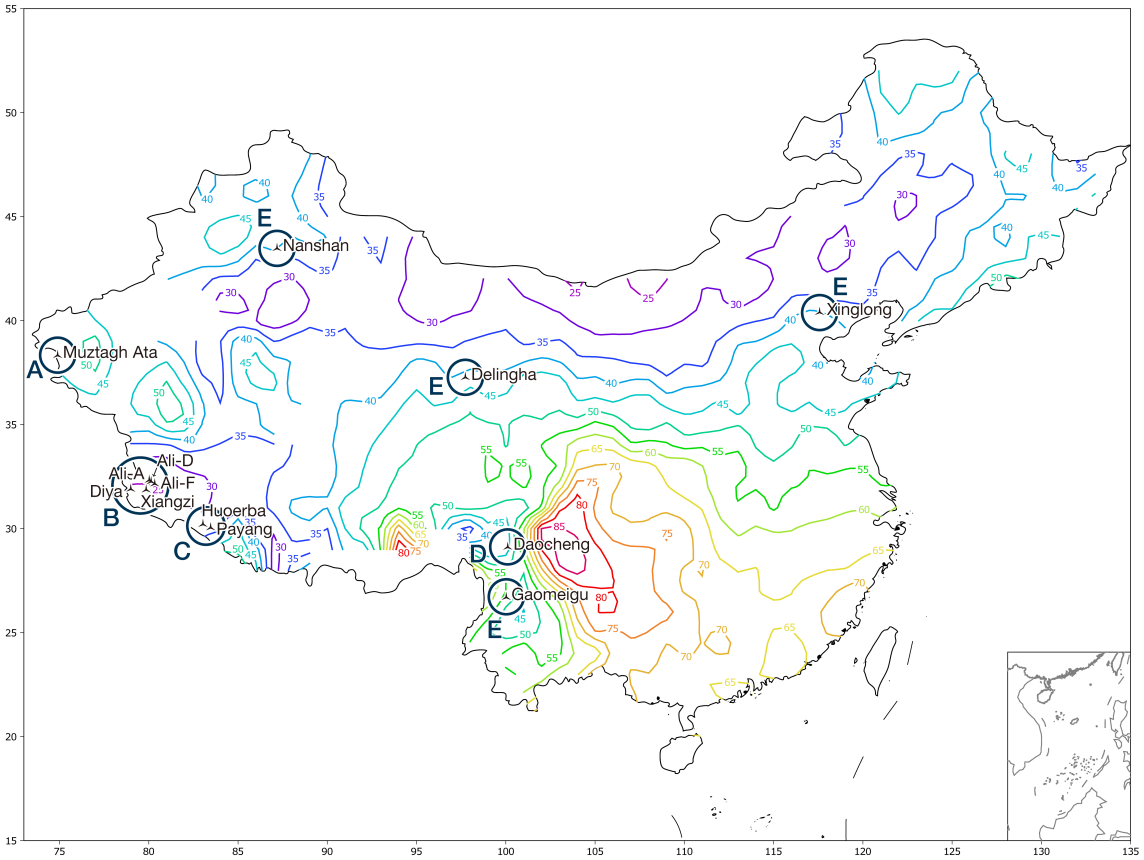

Fig. 1 The distribution of meteorological stations' cloud cover accumulated from 1961 to 2008. The data is from from the National Meteorological Information Center of China Meteorological Administration and includes 727 meteorological stations' climate data. The cloud cover observed by the naked eye, with a standard from 0 to 10, corresponding to the clear-sky and all-sky cloud with a stated accuracy of 10%, and directly converted the 0-10 naked-eye scale into a percentage. The cloud observations are performed four times a day, and the data at 2:00 AM in Beijing time is used for our nighttime cloud cover analysis. The abscissa represents longitude, and the ordinate represents latitude. The unit of a geographic location is degree. The marks on the contour lines represent the annual percentage of the night cloud cover. The location of sites and groups are plotted in the figure and listed in Table 1. (Reference to Qian et al. 2012)

2 CLOUD COVER BASED ON SATELLITE DATA

Meteorological satellites use specific cloud-sensitive spectral ranges (e.g., Ackerman et al. 1998; Frey et al. 2008) to measure radiation emitted or reflected by the Earth's surface or atmospheric systems on Earth (e.g., Menzel et al. 2008), and then to convert the measured radiation to cloud parameters. The inversion of cloud parameters generally has two steps: (1) cloud detection where cells are divided into cloud and clear sky cells, (2) parameter estimation where a variety of mathematical methodologies are used to infer cloud parameters (e.g., Barnes et al. 2016, Liu and Liu 2013).

While ground-based data will be vital for final site choices, meteorological satellite data can significantly reduce the requirement for site testing with ground-based observations and give a broad range of uniform measurements yielding multi-era cloud data. The long-time span of satellite data provides the possibility for in-depth analysis and study of cloud cover. Part of the International Satellite Cloud Characterization Program (ISCCP), GMS+MODIS, GMS+NOAA and MODIS-ST datasets are used in this study from 1996 to 2015 (e.g., Stubenrauch et al. 2013).

2.1 Cloud cover based on GMS+NOAA data

2.1.1 GMS+NOAA Data Description

The GMS satellite is a geosynchronous satellite, positioned at 140° E over the equator. The Stretched Visible and Infrared Spin Scan Radiometer (SVISSR) on the GMS consists of four channels, including visible (0.55–0.90 μm), near-infrared (1.628–1.625 μm), and infrared (10.5–11.5 μm and 11.5–12.5 μm) (Kramer 2002). The pixel resolution for GMS/SVISSR at infrared channels is 5 km at nadir (Dim 2007), and drops to the 20 km at the edge (Huang and Mao 1996).

NOAA satellites are polar-orbiting meteorological satellites. The 1st and 2nd generations of Advanced Visible and High-Resolution Radiometer (NOAA/AVHRR1 and NOAA/AVHRR2) on the NOAA consist of five channels, including (0.55–0.68 μm), near-infrared (0.725–1.10 μm and 3.55–3.93 μm), and infrared (10.3–11.3 μm and 11.5–12.5 μm), and the pixel resolutions at nadir for NOAA/AVHRR1 and NOAA/AVHRR2 are 1.1 km (Chen 2017).

The data presented in this paper were processed following the scheme devised by Huang and Mao (1996). The 90% pixels were processed by the time standard and the spatial standard from the ISCCP (Rodgers 1976) and the rest were processed by an appendix threshold standard defined by Huang and Mao (1996). In total 43,766 images from 1996 to 2004 were processed and provide 12 km resolution. Considering the GMS spatial resolution in western China is about 20 km, Mao (private communication) this data was conservatively binned the dataset by a factor of three to yield uniform 36×36 km^2 elements each supplied with a clear-night percentage based on the number clear hours divided by the total hours between the astronomical twilight.

2.1.2 GMS+NOAA Data Results

From GMS+NOAA data, there are four areas with high cloud cover marked in Fig. 2 and described in Table 2, centered on the Tibetan Plateau in western China. On a large scale, China has two main areas which are consistent with the historical ground-based observations and offering a high number of clear nights: (1) The vicinity of 40° N, extending from central Inner Mongolia to central Xinjiang. (2) The western and southwestern parts of the Tibetan Plateau from 78° E to 95° E. Two low cloud cover areas locate near 100° E. One is between Yunnan and Sichuan, with latitudes between 25° N and 30° N, the other is northern Qinghai, with latitudes ranging from 35° N to 40° N. Due to the topography, the potential area for astronomical sites in western Xinjiang to the Kazakhstan border is significantly reduced. However, we should note that GMS+NOAA data are not recent and have relatively low spatial resolution, which in a mountainous area may decrease

Table 2 Areas in western China with a low clear-night fraction based on GMS+NOAA

Mark	Region	Cause
1	The northwestern side of the Tibetan Plateau and the southern margin of the Tarim Basin.	From the Pamir wet area, the westerlies over the Pamir Plateau forms cloud, with the anticyclone circulation of the Tarim Basin (Dai 1990; Weng & Han 1998).
2	The eastern side of the Tibet Plateau, Sichuan, Yunnan, Guizhou.	A southwest low vortex system forms clouds, and the intersection of the southwest jet and the northwest jet produce weather systems (Liu et al. 2003).
3	The Great Bend of the Yarlung Zangbo.	From the Pamir wet area, combined with the water vapour from Yarlung Zangbo and the Indian Ocean, westerlies climb up and form cloud on the windward side (Liu et al. 2003).
4	The west side of the Tibetan Plateau.	From the Pamir wet area, westerlies climb up and form cloud on the windward side (Liu et al. 2003).

the accuracy of the specific site's cloud cover measurements. We note that the closest snow-covered mountain is 11 km from the Muztagh Ata site and so 36×36 km^2 resolution does not satisfy the cloud cover research for each site. Although, the work of Cavazzani et al. (2015) suggests that snow-cover is likely to significantly perturb the measurements it may not be indicative of a bad per se since for example the literal translation of Mauna Kea is White mountain in reference to its occasional snow covering. Therefore, higher resolution satellite data is needed.

2.2 Cloud cover based on MODIS data

2.2.1 MODIS Data Description

The Earth Observing System (EOS) project was started by the United States National Aeronautics and Space Administration (NASA) in 1999, including EOS/TERRA and EOS/AQUA satellites. The Moderate Resolution Imaging Spectroradiometer[1] (MODIS) of EOS/TERRA and EOS/AQUA has 36 spectral channels in the 0.4–14 μm across the visible and infrared regions. The resolutions at nadir depend on the channels, including 0.25 km for channels 1–2, 0.5 km for channels 3–7, and 1 km for channels 8–36 (Chen 2017). The polar-orbiting satellites EOS/TERRA and EOS/AQUA observe the earth four times a day at local times around 10:30 AM, 1:30 PM, 10:30 PM, and 1:30 AM (Platnick et al. 2003).

The National Meteorological Centre of China process the MODIS satellite data from January 1st, 2003 to December 31th, 2015. Based on it, we have statistics on the ratio of the cloudy-to-clear night. The information provided distinguishes specific resolution elements as either clear or cloudy. We count the number of cloudy-nights and divided the number of the days in that month or year, then get the monthly or annual percentages of cloudy nights. For easier comparison, we convert the percentages of cloudy-nights into clear-nights, which could result in an over estimation

[1] `https://modis-atmos.gsfc.nasa.gov/`

of the clear-night percentage if there is a difference in the assignment of cloudy/clear between EOS/TERRA and EOS/TERRA. We assume it is small for the clear-night rates of all sites higher than 50% from other satellite data based on the small differences of cloud cover from EOS/TERRA and EOS/TERRA results processed by Cavazzani et al. (2015) and Barnes et al. (2016).

2.2.2 MODIS Data Results

The annual percentage distribution of the cloudy-night from MODIS data from 2003 to 2015 is shown Fig. 2. Similar to the GMS+NOAA data, the percentage of cloud cover in the central and southeastern China is high, generally more than 50%. In the vicinity of 40° N, from the middle of Inner Mongolia to the middle of the Xinjiang Province, and west and the middle of Tibetan Plateau are low cloud cover areas. It is clear from the figure that each observatory is in a local low-cloud area, despite the different eras of site selection.

Comparing the cloud data of GMS+NOAA and MODIS, as shown in Fig. 2, there is a significant cloud reduction on the west side of 90° E in China, which might closely relate to the mechanism of the cloud formation. A large part of the humid air from the west side of 90° E is brought by the westerlies from the Pamir wet area (Dai 1990; Tian et al. 2004; Lioubimtseva et al. 2005). The Pamir wet area locates on the southwest side of the Pamirs, with its wet center near Kabul in Afghanistan and Islamabad in Pakistan. The westerlies move eastward, encountering the Iranian plateau, the Pamirs and the Tibetan Plateau. Due to the blocking effect of the mountains, the westerlies are divided into two branches, which are named the north branch of the westerlies and the south branch of the westerlies. The branch point locates at 60° E.

1. The north branch of the westerlies entering the Tarim Basin, converges near the Tibetan Plateau terrain boundary with anti-cyclonic circulation in the Tarim Basin. This effect resulted in a cloud system on the southwestern edge of the Tarim Basin, which is the cloud system near the Mutztag-ata site (group A).
2. The south branch of the westerlies moves along the Himalayas in the south of the Tibetan Plateau. When the jet is strong, it will rise to the high altitudes of the Himalayas. This effect results in the clouds around the Xiangzi, Diya, Ali-F, Ali-D, Ali-A, Huoerba, and Payang (group B and C).

The water vapor situation in the Pamir wet area is changing over a long period. According to the study of the Intergovernmental Panel on Climate Change (IPCC), during the 21st century, the inland regions showed gradual trend of increasing drought, especially in subtropical, low latitudes and mid-latitudes. More specific observations show that in Afghanistan and Pakistan, the annual precipitation from 1979 to 2005 showed a significant decline compared to the average annual precipitation from 1961 to 1990. In our data the change can be seen when comparing the GMS+NOAA data from 1998 to 2003 in the higher panel of Fig. 2 with the MODIS data from 2004 to 2015 plotted on the same scale in the lower panel of Fig. 2. Furthermore, based on the SRES A1B scenario, "fifteen-model" shows the water vapor supplied by the Pamir wet area will significantly reduce, which results in cloud reduction. In all areas impacted by westerlies, the future cloud formation

rate will be lower (Bates et al. 2008). From MODIS data, the monthly percentage distribution of the cloudy-nights accumulated from 2003 to 2015 is shown in Fig. 3. Each subgraph represents the percentage distribution of cloudy-night at each month and all of them were arranged following the seasonal order, started with March in spring. Most of China is dominated by the East Asian Summer Monsoon. The warm and humid air from the tropical sea area is abundant in summer, with the high temperature and extensive evaporation giving rise to a period of excessive summer cloud. The monthly average cloud cover in the southeastern and central parts of China is generally higher than 50% durning the night. Due to the lower humidity, the night-time cloud cover from central Inner Mongolia to central Xinjiang and most of Tibet remains at a low level and varies little with the seasons. The cloud cover of the sites in group D is also higher in summer, and lower in winter. Although this phenomenon is the case in most parts of southeastern China, the cloud formation is mainly impacted by the India Monsoon in this area. The significant seasonal changes of clear-nights percentages in each site are shown in Fig. 4, and the main reason for the changes in western China is the combination of the westerlies and the monsoons. The wind system in China is shown in Fig. 5, which transports the water vapors to condense into clouds under appropriate conditions. For westerlies in China, the strength and location are closely related to the season. In winter, the westerlies are stronger and southerly, with the main direction around the vicinity of 30° N. In summer, the westerlies are weaker and northerly, with the main direction around the vicinity of 40° N (Yi 2011). Therefore, the sites affected by the westerlies have more cloud in winter.

For monsoons in China, the condition is more complex. Three types of monsoons affect the Chinese climate, including the Winter Monsoon from Mongolia, the East Asian Summer Monsoon from the Pacific Ocean, and the Indian Monsoon. Warm and humid water vapor in the eastern Indian Ocean passes through the Bay of Bengal and crosses the Yarlung Zangbo to the east of the Tibetan Plateau and is the main element to generate clouds in the western part of China. In the summer, the monsoons winds are stronger, while in the winter, the monsoons winds are weak. Thus, the sites affected by the monsoons have more cloud in the summer.

The influence of the westerlies and monsoons can be analyzed in the statistics of the clear-sky percentages of each site. Limited by the wind strength and distribution of the westerlies and monsoons, the sites in the northwest are susceptible to the westerlies, while sites in the southeast are susceptible to the monsoons. Therefore, in group order A, B, C, and D are decreasingly effected by the westerlies and increasing affected by monsoon. Assuming that the conditions for cloud formation from water vapor in each region remains unchanged, the cloud cover increase in February can be regarded as a sign of the westerlies influence, and the cloud cover increase in August is a sign of the monsoon influence. At the same time, the degree of cloud cover could be regarded as a sign of the degree of the westerlies or monsoon influence. This is illustrated by the spatial distribution of the cloud cover in February and August (Fig. 6∼7), and the statistics in Fig. 4. As shown in Fig. 8, group B (in the case of Ali-F, 80.33494° E, 5,125 m) and C (in the case of Payang, 83.46912° E, 4,600 m) are located north of Himalayas and south of Gangdese, with longitudes between 78° E

and 84° E and altitudes between 4,621 and 5,292 m. However, group B and C present significantly different seasonal cloud distributions from the MODIS data. The water vapor situation of group B is more impacted by the westerlies and less by the monsoons; group C sites are almost not affected by the westerlies and mainly by the monsoons. We infer a difference in the cloud formation in the area north of the Himalayas between the east and west side of 82° E.

The most significant landmark near 82° E is Mayum La (marked in Fig. 8), with the longitude of 82.43429° E and the latitude of 30.63046° N, which is marked as a bold black line in Fig. 8. It is the watershed between the sources of the Brahmaputra and Indus rivers. The altitude of Mayum La is 5,285 m, significantly higher than the average local elevation and appears to significantly weaken the influence of the monsoons from the west. Thus on the west side of Mayum La, the cloud formation is more affected by the westerlies, on the other hand, on the east side it is dominated by the monsoons. When we make comparison with the GMS+NOAA data, a new cloud strip (marked in Fig. 6 by a black arrow) formed near group B and C in the MODIS data, which distributes in the Gangdese. The cloud strip is evident in winter and disappears in summer, which suggest its formation is effected by the westerlies. Considering the spatial distribution of the GMS+NOAA's annual average cloud cover in Fig. 2, the clouds on the west side of the Tibetan Plateau have accumulated in large numbers and have not crossed the Himalayas into China. We can speculate that the westerlies have significantly enhanced since 2003. This phenomenon is consistent with the IPCC's Fourth Assessment Report, which concluded that mid-latitude westerlies have generally increased in both hemispheres (Stocker et al. 2013).

The annual average percentages of clear-nights from 2003 to 2015 are shown in Fig. 9. The data from the A, B, C, D groups are more cloud-free than the currently running observing stations in group E. From Table 4, the annual average cloud cover of the sites in group C is the lowest, group B and A are higher than group D. Group A has the most stable annual average cloud cover, On the other hand, the difference between the highest and lowest in group B is significant, and the standard deviation of group B is 3.31, though it also has the largest number of sites. Aside from a possible slight improvement in clear skies at group C, we note that Fig. 10 does not illustrate any particular evidence for any overall trend in site characteristics that might be expected based on Section 2.2. Our analysis suggests that this has a local explanation in that that while the overall level of cloud has gone down somewhat this has been compensated by increased seasonality introduced by local features such as that illustrated in Fig. 6. As expected the performance of the sites will be related to the local geographical features. For comparison between the sites in China and TMT/ELT sites, a team from Institute of Geography Sciences and Natural Resources Research, Chinese Academy of Sciences processed the MODIS data (CAS MODIS for short) from 2003 to 2014 at eight sites by a different method (Liu & Liu 2013). This method estimates if the pixel is with cloud or not and then makes further cloud sub-divisions.

Liu and Liu's (2013) sub-divisions include a "thin cloudy" assignment though it appears that this subdivision is rather sensitive and should be interpreted with caution. In particular, there maybe one or more issues in the ability of the data processing to robustly identify thin cloud: (1)

the variable "Angle R37" is overestimated or the parameter of "Reference R37" is underestimated in the workflow of the Liu and Liu (2013), (2) the sites are relatively small in comparison with the spatial resolution of the satellite data and topographic features of these sites are different from those of their surroundings will be different and so local details need to be checked.

The CAS MODIS "clear" fractions for Mauna Kea and Armazones are less than has been found by a number of long-running experiments. The geographical feature of the sites, including near the ocean (Cavazzani et al. 2011), covered by snow, low altitude mist will impact results. In certain conditions such features can introduce a cloud cover difference of more than 75% (Cavazzani et al. 2015). This explanation seems particularly plausible in the case of Mauna Kea given its more varied local geography and climate. If we ignore the CAS MODIS sub-divisions between "clear" and "thin cloudy", the simplified result is more reasonable. We plot this data in Fig. 10, and put "clear" and "thin cloudy" in the same bin with the same color. We compared the combination of "clear" and "thin cloudy" with the "clear" data from the National Meteorological Centre of China (NMC MODIS for short), we find that NMC MODIS and so-called "simplified CAS MODIS" are relatively consistent with an average difference of 2% (see Table 3). It can be seen that the simplified CAS MODIS data are very close to cloud-free night percentages found by Barnes et al. (2016) and Cavazzani et al. (2017) from the MODIS data.

From the simplified CAS MODIS data, the Muztagh Ata from group A, Ali-A and Diya from group B, Payang from group C, and Daocheng from group D are all slightly lower than the TMT/ELT sites and higher than the Xinglong Observatory. The annual average percentages of cloud-free nights from MODIS dataset, including NMC MODIS, CAS MODIS, the MODIS processed by Barnes et al. (2016), and the MODIS processed by Cavazzani et al. (2017), listed in Table 3 and Table 4 and show reasonably consistency with each other. Barnes et al. noted that the cloud detection algorithm may over-rely on surface temperature retrievals from MODIS, and there may be a bias in the nighttime cloud cover frequency data toward lower-than-actual cloud cover frequency. In other words, we should regard the Table 4 and Fig. 11 as representing the maximum percentage of clear nights that might be obtained.

3 CONCLUSION

In our consideration of suitable astronomical sites in western China, from a meteorological perspective we took into account four low cloud areas around the Tibetan Plateau, including: the northwestern side of the Tibetan Plateau and the southern margin of the Tarim Basin; the eastern side of the Tibetan Plateau, Sichuan, Yunnan, Guizhou; the Great Bend of the Yarlung Zangbo; the west side of the Tibetan Plateau. These result in seasonal changes in the cloud in western China and changes influenced by the westerlies and monsoons. We find evidence for the cloud cover reducing in areas affected by the westerlies, which is consistent with the expectations from climate change models.

We identified three groups of sites A, B, and C with significant advantages:

Table 3 The annual average percentage of clear free nights from NMC MODIS, CAS MODIS, Barnes et al. (2016) MODIS, and Cavazzani et al. (2017) MODIS for all sites referred in this work. We give the historical meteorological station data in italic so as to note that this data has been recorded in a non-digital format and so will have different biases. The data from Barnes et al. is from the contour plot in their Fig. 2(c) and (d) and private communication. The data from Cavazzani et al. MODIS is given in italic since inferred from the Table 3. and Fig. 7. It should noted that the diversified definitions of "clear" fraction were used here due to the methods used, and it should not be confused with the fraction of photometric nights or the time an observatory can be used at the sites. The relationship with the all-sky camera is discussed by Cao (2019).

Group	Site	NMC	CAS	Barnes	Cavazzani
	Epoch	2003 – 2015	2003 – 2014	2001 – 2011	2003 – 2015
A	Muztagh Ata	77.8	78.1	-	-
B	Xiangzi	80.2	-	-	-
B	Diya	89.1	84.2	-	-
B	Ali-F	83.8	-	-	-
B	Ali-D	81.8	-	-	-
B	Ali-A	86.8	82.6	-	-
C	Payang	86.6	82	-	-
C	Huoerba	89.0	-	-	-
D	Daocheng	71.1	71.6	-	-
E	Delingha	74.1	-	-	-
E	Gaomeigu	66.9	-	-	-
E	Nanshan	70.7	-	-	-
E	Xinglong	67.9	68.5	-	-
-	Mauna Kea	-	84.1	88%(TERRA)/84%(AQUA)	-
-	Armazones	-	85.5	-	*87.5*

Table 4 Comparison of annual average percentage of cloud-free nights from NMC MODIS and "simplified CAS MODIS" data processing.

Group	NMC	CAS
A	77.2	78.1
B	84.3 ± 3.6	83.4
C	87.8 ± 1.7	82
D	71.1	71.6
E	70.1 ± 3.2	68.5

Group A locates in the Eastern Pamirs, a series of peaks on the east side of the site, including Kongur Tagh (7,719 m), Kongur Tiube (7,555 m), and Muztagh Ata (7,546 m) though we have only considered the later of these. The water vapor brought into the Tarim Basin by the westerlies is blocked by these peaks on the east of the site, and leads to a reasonably consistent amount of clear-sky throughout the year.

Groups B and C are located at the southwest of the Tibetan Plateau, between the Gangdese and Himalayas, which avoids the unstable air areas caused by high-pressure and low-pressure systems and the winds caused by momentum exchange between high-level and low-level air (Huang & Mao 1994). The area near group C has excellent cloud statistics in this study. However, this area is

vulnerable to the negative impact of a potentially expanding of the monsoon region due to climate change visible in a reduced fraction of clear-sky in August and surrounding months.

On the whole, the clear nights available in groups A, B, and C (∼83% on average) are slightly lower than the TMT/ELT sites (∼85% on average) and higher than the operational observatories in China (<70% on average). Further analysis of satellite data and its detailed comparison with ground-based data are required and presented elsewhere in this special edition (e.g., Cao et al. 2019).

The cloud cover from satellite depends on data sources and their processing algorithms: different instruments observing in specific band reveal various physical characteristics of the cloud; even with identical original data, results interpreted by different algorithms would vary as well. After data analysis and comparison, the results are acceptable in the long-term cloud cover study. Moreover, as mentioned before, the ground-based observation are essential in candidate sites.

ACKNOWLEDGEMENTS

We are very grateful to Jie-Tai Mao for satellite data processing and Mallory Barnes for clarifying details of Barnes et al. The research is partly supported by the Operation, Maintenance and Upgrading Fund for Astronomical Telescopes and Facility Instruments, budgeted from the Ministry of Finance of China (MOF) and administrated by the Chinese Academy of Sciences (CAS).The research is also supported by the National Natural Science Foundation of China (NSFC) under No. 11573054, 11703065, 11603044, and 11873081. The MODIS data referred in this research were provided by the teams from the National Meteorological Centre of China and the Institute of Geography Sciences and Natural Resources Research, Chinese Academy of Sciences. HRAJ acknowledges support from a CAS PIFI and UK STFC grant ST/R006598/1.

References

Ackerman, S. A., Strabala, K. I., Menzel, W. P., et al. 1998, Journal of Geophysical Research: Atmospheres, 103(D24), 32141-32157

Barnes, M. L., Miura, T., & Giambelluca, T. W. 2016, Journal of Climate, 29(1), 77-90

Bates, B., Kundzewicz, Z., & Wu, S. 2008, Climate change and water (Intergovernmental Panel on Climate Change Secretariat)

Cavazzani, S., Ortolani, S., Zitelli, V., & Maruccia, Y. 2011, MNRAS, 411(2), 1271-1283

Cavazzani, S., Zitelli, V., & Ortolani, S. 2015, MNRAS, 452(2), 2185-2194

Cavazzani, S., Ortolani, S., Zitelli, V. 2017, MNRAS, 471, 2616–2625

Chen, W. 2017, Weixing Qixiangxue, Satellite meteorology (3rd ed.) (China Meteorological Press)

Cui, X., Zhu, Y., Liang, M., et al. 2018, Introduction on Chinese 12m optical/infrared telescope (LOT). In Ground-based and Airborne Telescopes VII (Vol. 10700, p. 107001P). International Society for Optics and Photonics

Chen, D., Wang, J. C., Xu, J., et al. 2003, Publications of the Yunnan Observatory, 95, 1-7

Dai, J. 1990, Qingzanggaoyuan Qihou, The climate of Qinghai-Tibet Plateau (China Meteorological Press)

Dim, J. R., Takamura, T., Okada, I., Nakajima, T. Y., & Takenaka, H. 2007, Journal of Geophysical Research: Atmospheres, 112(D13)

Frey, R. A., Ackerman, S. A., Liu, Y., et al. 2008, Journal of Atmospheric and Oceanic Technology, 25(7), 1057-1072

Huang, Y., & Mao, J. 1994, Chinese Journal of Astronomy and Astrophysics, 14, 379-384

Huang, Y., & Mao, J. 1996, Astrophysics reports (Pub. Beijing Astronomical Observatory), 28, 62-96

Kramer, H. J. 2002, Observation of the Earth and its Environment: Survey of Missions and Sensors (Springer Science & Business Media)

Lioubimtseva, E., Cole, R., Adams, J. M., & Kapustin, G. 2005, Journal of Arid Environments, 62(2), 285-308

Liu, H., Zhu, W., Yi, S., et al. 2003, Acta Meteorologica Sinica, 61(4), 465-473

Liu, J., Zhang, Y., Feng, G., & Bai, C. 2013, Proceedings of the International Astronomical Union, 9(S298), 427-427

Liu, R., & Liu, Y. 2013, Remote Sensing of Environment, 133, 21-37

Melnick, J., & Monnet, G. 2011, Revista Mexicana de Astronomía y Astrofísica, 41, 36-41

Menzel, W. P., Frey, R. A., Zhang, H., et al. 2008, Journal of Applied Meteorology and Climatology, 47(4), 1175-1198

Platnick, S., King, M. D., Ackerman, S. A., et al. 2003, IEEE Transactions on Geoscience and Remote Sensing, 41(2), 459-473

Qian, X., Yao, Y. Q., & Zhang, Y. J. 2012, Acta Astronomica Sinica, 53, 426

Rodgers, C. D. 1976, Reviews of Geophysics, 14(4), 609-624

Schöck M., et al. 2009, PASP, 121, 384

Schöck, M., Nelson, J., Els, S., et al. 2011, Revista Mexicana de Astronomía y Astrofísica, 41, 32-35

Stocker, T. F., Qin, D., Plattner, G. K., et al. 2013, Climate change 2013: The physical science basis (Cambridge University Press)

Stubenrauch, C. J., Rossow, W. B., Kinne, S., et al. 2013, Bulletin of the American Meteorological Society, 94(7), 1031-1049

Tian, H., Guo, P., & Lu, W. 2004, Journal of tropical meteorology, 20(4), 401-408

Tian, J. F., Deng, L. C., Zhang, X. B., et al. 2016, Publications of the Astronomical Society of the Pacific, 128(968), 105003

Weng, D., & Han, A. 1998, Journal of Applied Meteorological Science, 9(1), 32-37

Yi, S. 2011, Holocene vegetation responses to East Asian monsoonal changes in South Korea. In J. Blanco & H. Kheradmand (Eds.), Climate Change-Geophysical Foundations and Ecological Effects (IntechOpen)

Zhang, J. C., Ge, L., Lu, X. M., et al. 2015, Publications of the Astronomical Society of the Pacific, 127(958), 1292

Zhang, Y., Wang, P., & Yao, Y. 2010, Scientia Sinica (Physica,Mechanica & Astronomica), 40(10), 1302-1314

This manuscript was prepared with the RAA LaTeX macro v1.2.

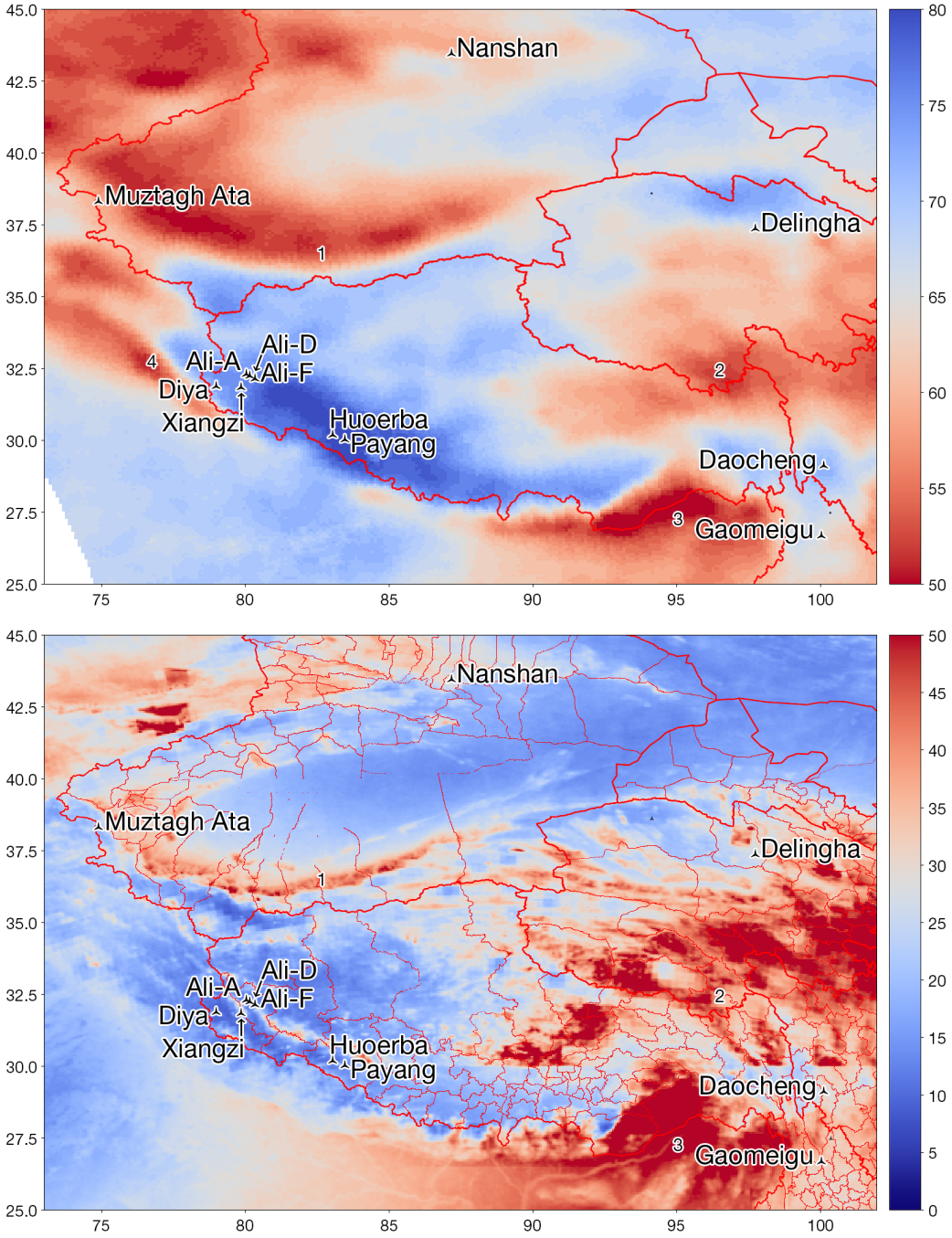

Fig. 2 The percentage distribution of GMS+NOAA clear nights accumulated from 1996 to 2003 for western China is in the higher panel of the figure. The abscissa represents longitude, and the ordinate represents latitude. The color scale is from 50 to 80 chosen to easily distinguish the most promising regions. The thick red lines denote the country borders, the thinner red lines mark provincial and city borders and the thin red lines are rivers. The percentage distribution of cloudy-night less than 50% accumulated from January 1st, 2003 to December 31st, 2015 for national and western China from MODIS data is in the lower panel of the figure. The abscissa represents longitude, and the ordinate represents latitude. The borders are roughly aligned with GMS+NOAA data, moreover, the colors scale is from 0 to 50 and are chosen so as to optimize visual comparison with the GMS+NOAA data.

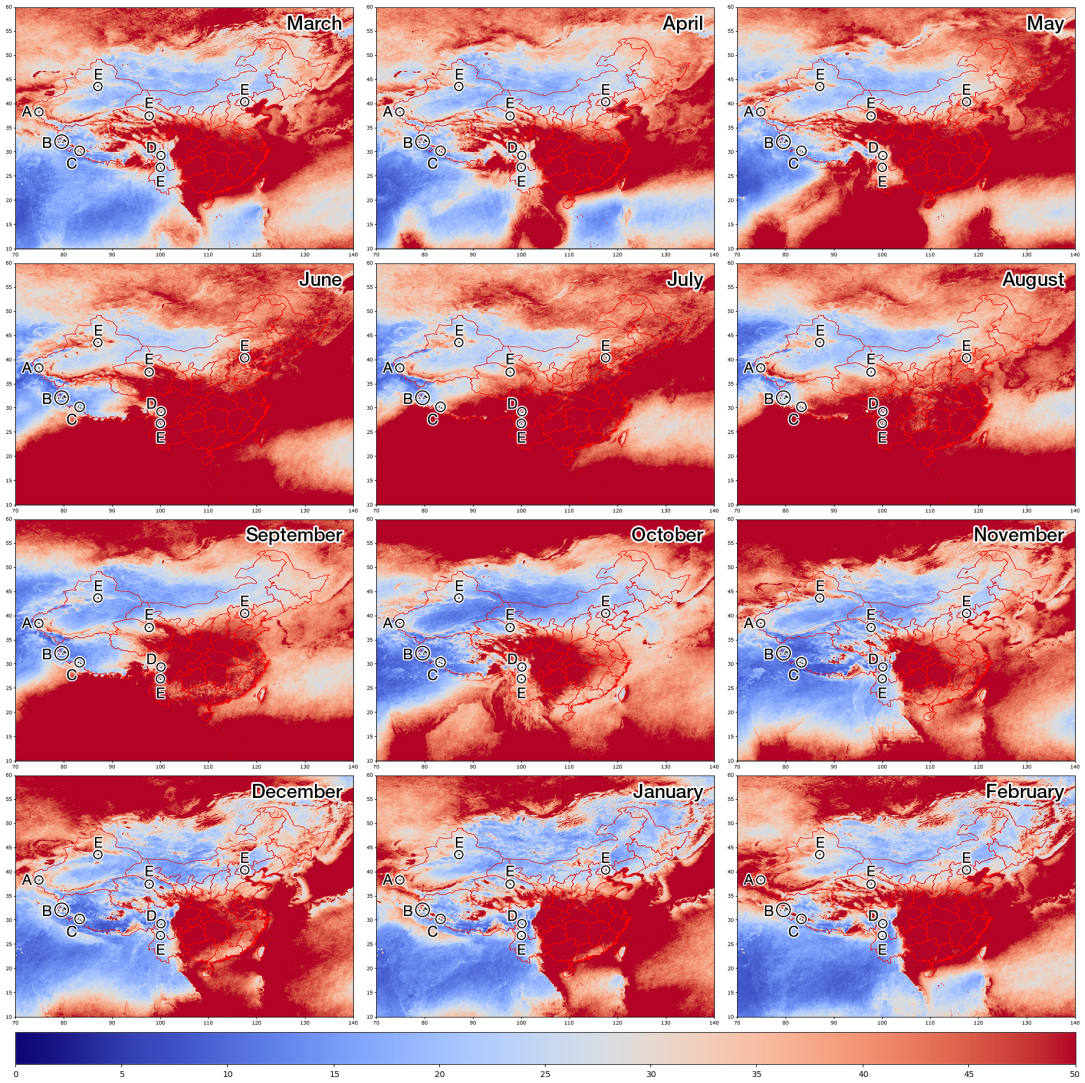

Fig. 3 The MODIS monthly percentage distribution of cloud cover less than 50% accumulated from January 1st, 2003 to December 31th, 2015.

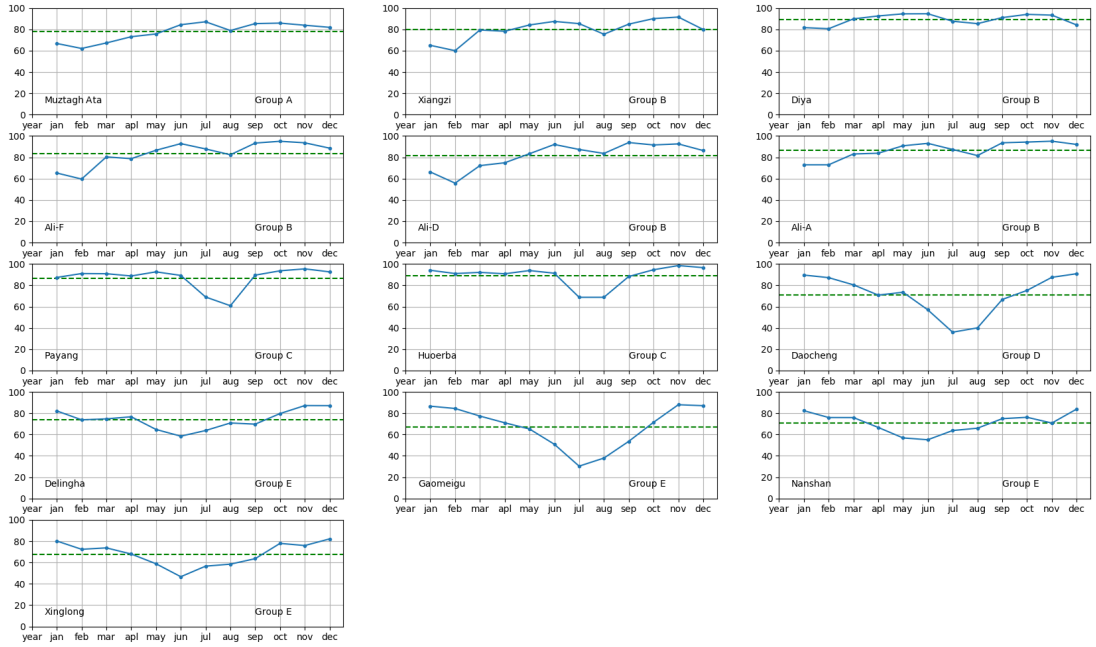

Fig. 4 Annual trends of MODIS clear-nights percentage accumulated from January 1st, 2003 to December 31th, 2015. Each point represents a month average percentage of cloud cover.

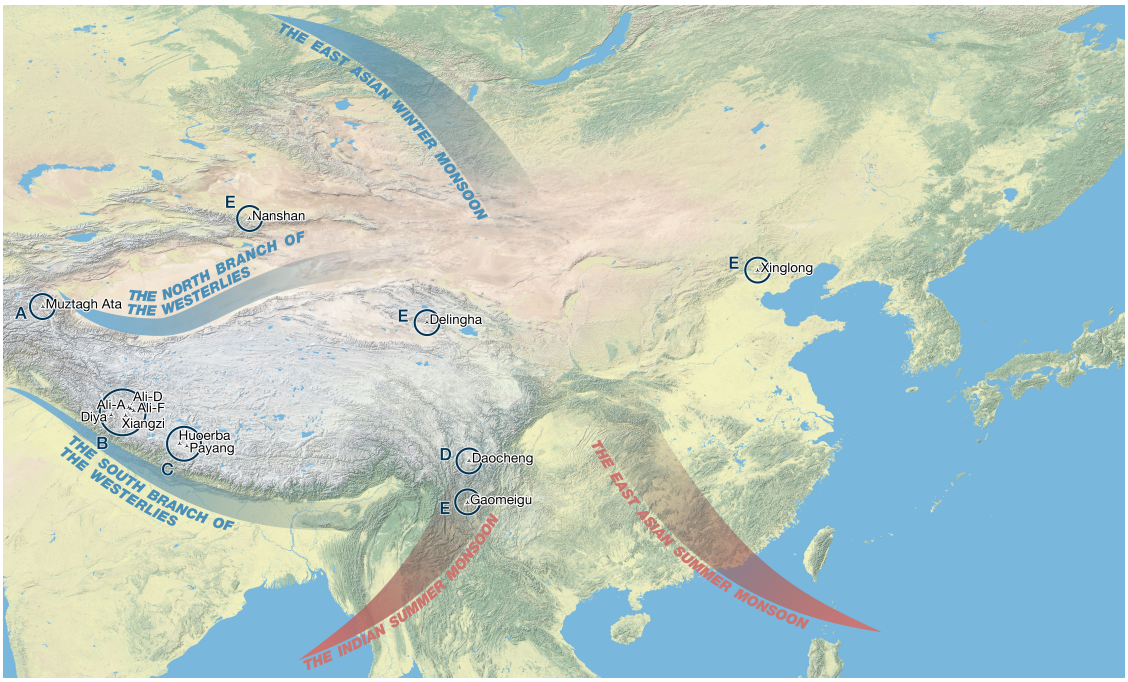

Fig. 5 The geographical distribution of westerlies and monsoons. The winds with blue prevail in winter, and the winds with red prevail in summer.

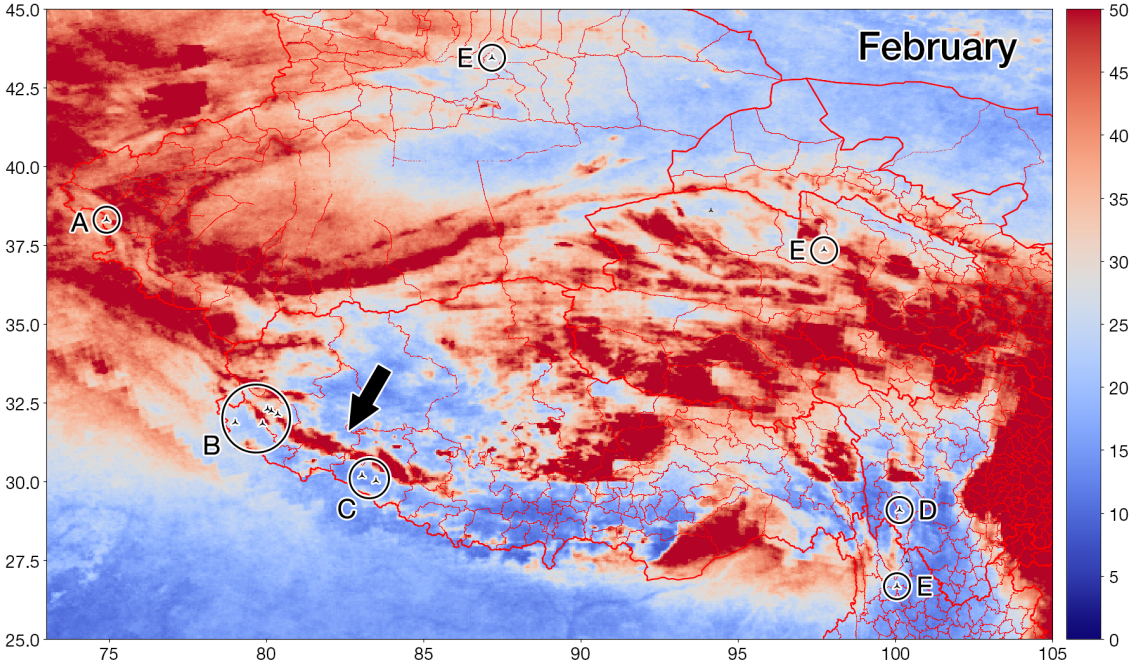

Fig. 6 The MODIS monthly percentage distribution of cloud cover less than 50% in western China in February. The black arrow presents a new cloud strip, not seen in GMS+NOAA.

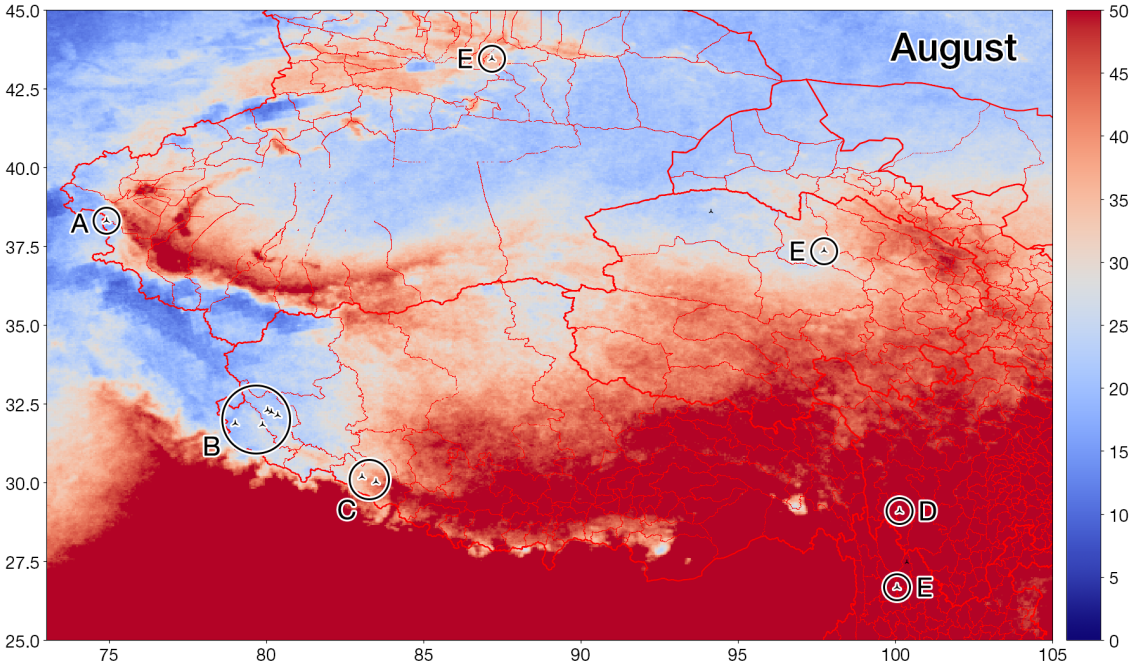

Fig. 7 The MODIS monthly percentage distribution of cloud cover less than 50% in western China in August.

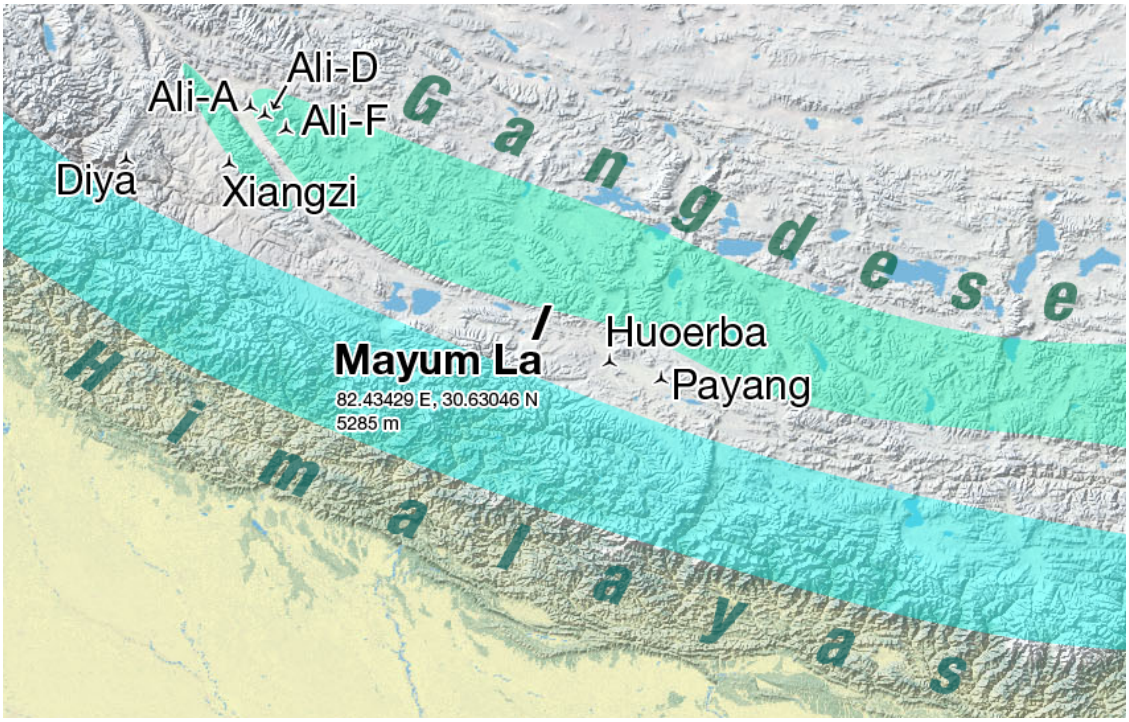

Fig. 8 The location of the Mayum La. The colors with cyan and light turquoise represent the rough geographical distributions of the parts of the Himalayas and Gangdese. Blue color represent lakes.

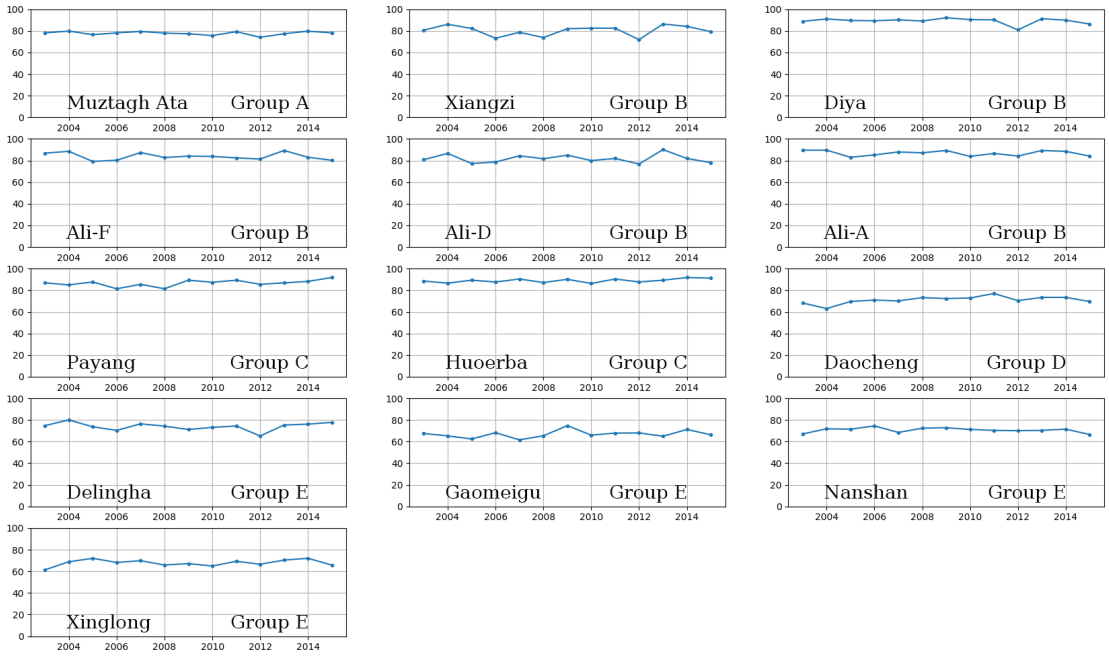

Fig. 9 The MODIS annual average percentages of clear-nights from January 1st, 2003 to December 31th, 2015.

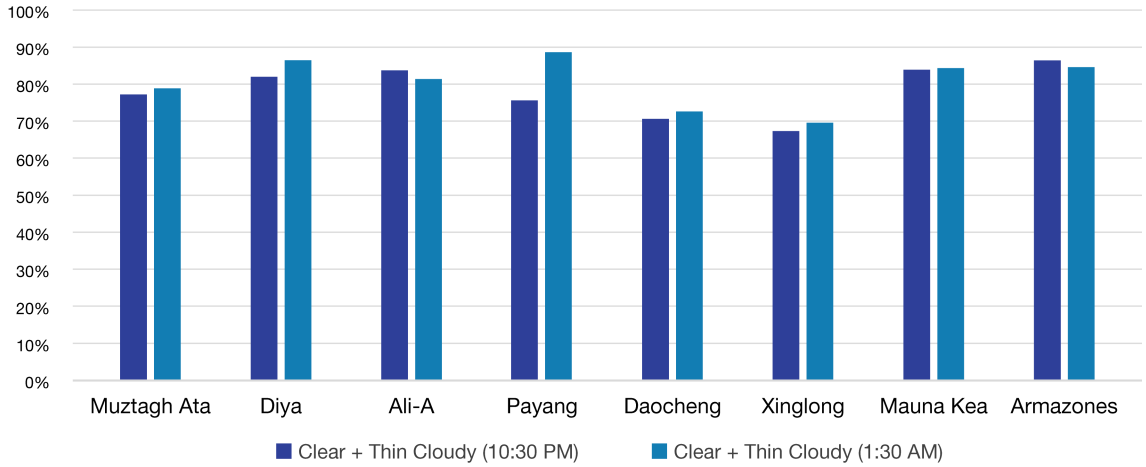

Fig. 10 The possibility of clear and thin cloudy at 10:30 PM and 1:30 AM (in local time) from CAS MODIS. The definition of the clear and thin cloudy is from Liu and Liu (2013).